PAPER

Concentration dependent pathways in spontaneous self-assembly of unilamellar vesicles†

Jérémie Gummel,[a] Michael Sztucki,[a] Theyencheri Narayanan*[a] and Michael Gradzielski[b]

We report on the structural dynamics underlying the formation of unilamellar vesicles upon mixing dilute solutions of anionic and zwitterionic surfactant solutions. The spontaneous self-assembly was initiated by rapid mixing of the surfactant solutions using a stopped-flow device and the transient intermediate structures were probed by time-resolved small-angle X-ray scattering. The initial surfactant solutions comprised of anionic lithium perfluorooctanoate and zwitterionic tetradecyldimethylamine oxide, where the mixtures form unilamellar vesicles over a wide range of concentrations and mixing ratios. We found that disk-like transient intermediate structures are formed at higher concentrations while more elongated forms such as cylinder-like and torus-like micelles are involved at lower concentrations. These differences are attributed to monomer addition mechanism dominating the self-assembly process when the initial concentration is well below the critical micellar concentration of the anionic surfactant, while at higher concentrations the process is governed by fusion of disk-like mixed micelles. This means that the pathway of vesicle formation is determined by the proximity to the critical micellar concentration of the more soluble component.

1. Introduction

Unilamellar vesicles (ULVs) are of great practical interest due to their potential use in nano- and biotechnology for encapsulation and delivery of cargo molecules.[1–3] Applications include detergents, pharmaceuticals, food products, *etc.*[4,5] From a fundamental point of view, ULVs are thought to be an idealistic representation of a cell membrane.[3] As a result, extensive studies have been carried out to describe their structures in equilibrium.[6–8] Nevertheless, transient intermediate structures occurring in their formation process or morphological transitions are only beginning to be explored.[9–12] Understanding the pathways of self-assembly is the key to achieve control and predictive capabilities in the bottom-up approach of fabricating well-defined nanostructures.[1,2] This applies in particular to vesicle systems, which in many cases are non-equilibrium systems.[1,2,13]

Experimentally, there are different ways of initiating the self-assembly of amphiphilic molecules to form ULVs.[1,2,8] Most well studied systems are surfactants[6,7,10–12,14–16] and block copolymers[17–19] in selective solvents. The self-assembly process can be induced by rapid mixing of oppositely charged surfactant solutions,[6,10,15,20] temperature[19,21,22] or pH jumps.[23,24] The process of

formation of ULVs usually involves different stages with certain rate limiting steps, making the kinetics spanning from milliseconds to days, depending on the type of amphiphiles employed and the type of transformation taking place.[25,26] Among the different ways to form ULVs *in situ*, the rapid mixing of two oppositely charged surfactants is a convenient approach to probe the kinetic pathway of the self-assembly process.[27–30] Two surfactant solutions can be mixed efficiently within a millisecond using the stopped-flow method and the structural evolution of the system can be followed by means of time-resolved small-angle X-ray scattering (SAXS) or neutron scattering (SANS).[29] Thanks to the high brilliance X-ray sources, such structural kinetic experiments can be performed with millisecond time resolution and structural resolution in the sub-nm range.[28,30,31] In addition, there has been significant progress in the computer simulations[26,32–34] of the pathways of these self-assembly processes but a direct comparison between experiments and simulations is still lacking to date.

In general, long time stable ULVs can be generated in appropriately chosen catanionic[6,7,10,11,35–37] or zwitteranionic surfactant mixtures.[8,14,15,20] In this work, we have used anionic surfactant, lithium perfluorooctanoate (LPFO) and zwitterionic surfactant, tetradecyldimethylamine oxide (TDMAO). Previous investigations have shown that in this system vesicles are formed over an extended mixing range for a relative mole fraction of TDMAO, x[TDMAO], of 0.15–0.7,[38,39] due to the stiffness of the perfluorinated chains. This system has been studied extensively to unravel the pathways of ULV self-assembly but then the focus was on the concentration range well above the critical micellar

[a]ESRF, 6 rue Jules Horowitz, F-38043 Grenoble, France. E-mail: narayan@esrf.eu

[b]Technische Universität Berlin, D-10623 Berlin, Germany

† Electronic supplementary information (ESI) available: Two pathways for self-assembly of unilamellar vesicles in zwitter–anionic surfactant mixtures depending on the proximity to the cmc of more soluble component. See DOI: 10.1039/c1sm05354j

concentration (cmc) of both micelles.[14,15] In this work, we have investigated surfactant concentrations around and well below the cmc of the LPFO but above the cmc of the TDMAO. This change of concentration significantly modifies the starting conditions and thereby the pathway of the self-assembly process, leading to new intermediate transient structures as well as different time scales for the intermediate steps. Indeed, vesicle and bilayer systems are known for their propensity to form different structures depending on their preparation history.[40] In that context our findings are very relevant as they show how the pathway of self-assembly processes can vary largely depending on the starting conditions, which is of importance for many questions regarding formulation with surfactants and their applications.

2. Materials and methods

2.1 Materials

The initial solutions consisted of 50 mM aqueous solutions of TDMAO and LPFO as in the previous work.[14] TDMAO was a gift from Clariant and was purified by crystallization from ether/ethanol solution. LPFO was obtained from Fluka and recrystallized from ether. The cmc's of TDMAO and LPFO are 0.12 mM and 31 mM, respectively.[38] From the 50 mM stock solution, dilute solutions of both surfactants were prepared using deionized milliQ water. Here the results obtained from 25 mM and 8 mM surfactant solutions are presented which illustrate two distinctly different pathways of ULV formation. Both concentrations 25 mM and 8 mM are either just or well below the cmc of LPFO but well above that of TDMAO.

2.2 Stopped flow device

The fast mixing of the surfactant solutions was realized by a stopped-flow mixing device described elsewhere.[28] The mixing apparatus is based on a commercial stopped-flow device (SFM-400) from Bio-Logic (Claix, France). It consists of four motorized syringes interconnected through three mixers. The exit of the last mixer is coupled to the scattering cell which is fabricated from a quartz capillary of diameter about 1.5 mm and wall thickness of about 10 μm. The flow is stopped by a hard-stop which consists of a solenoid valve placed at the end of the flow line and it is activated at the termination of the mixing sequence. The dead time of the device is primarily determined by the time to transfer the mixture from the last mixer to the beam crossing point on the capillary cell. This transfer time is about 2.2 ms for a flow rate of 6.7 ml s^{-1} while the turbulent mixing time is of the order of 0.1 ms.[28] This means that the earliest time scale probed is about 2.3 ms. The dead time and the quality of mixing are verified using the procedure described previously.[28]

2.3 Time-resolved small angle X-ray scattering

SAXS measurements were performed at the ID02 beamline at the European Synchrotron Radiation Facility in Grenoble, France.[28] The sample-to-detector distance was 2.5 m and X-ray wavelength (λ) was 0.1 nm corresponding to a q (magnitude of the scattering vector) of 4×10^{-2} to 2 nm^{-1}. The combination of high brilliance of the beam (~5×10^{13} photons per s) and high sensitivity of the

CCD detector (FReLoN 4M) allowed us to obtain sufficient intensity statistics with an acquisition time of 5 ms which is defined by the opening of a high precision tandem X-ray beam shutter. In addition, the incident and transmitted beam intensities were simultaneously recorded. However, the CCD detector has a readout time of about 140 ms. In order to fill this readout gap, a sequential data acquisition scheme was employed. The SAXS detector, tandem shutter, beam intensity measurements were synchronized by a time-frame generator which in turn was triggered by a hardware signal from the stopped-flow device. Typically, the stopped-flow mixing sequence involved a slow mixing phase (lower flow rates, ca. 2 ml s^{-1}) in which the flow lines are refreshed, i.e. old remaining solution is flushed out, and a subsequent fast mixing phase. The data acquisition cycle (involving about 100 frames) was triggered at the beginning of the fast mixing phase and the solenoid hard-stop was activated at the end of this phase. The first 5 ms frame is placed towards the end of the fast mixing phase such that the kinetic time is equal to the dead time (2.3 ms) of the stopped-flow device and the system ages after the cessation of flow. In the sequential data acquisition scheme, the first frame of the next cycle is delayed by a desired time (typically 10 ms). By repeating the cycle 5–6 times with progressive increase in the initial delay time, the readout time gap of the CCD detector can be adequately covered. Of course, this approach relies on the kinetic reproducibility of the self-assembly process. It was verified that indeed is the case with the systems studied here.

Measured two dimensional scattering patterns were normalized to an absolute intensity scale after applying the detector corrections for spatial homogeneity and linearity. Normalized SAXS patterns were azimuthally averaged to obtain the one dimensional scattering profiles as a function of time. Both sample and background (water) measurements were done at the same spot on the stopped-flow capillary cell to ensure an accurate subtraction of the background. In order to obtain a good background scattering curve, multiple frames (20) were acquired and averaged after normalization and azimuthal integration. In the following, the scattered intensity after the subtraction of the background is represented by I(q). All measurements were performed at a temperature of 22 °C. For static measurements, surfactant solutions were contained in a flow-through capillary cell with the same diameter as the stopped-flow cell.

2.4 Data analysis

The background subtracted normalized scattered intensity is directly related to the morphology and interaction between micellar objects in the scattering volume.[41] The I(q) from a particulate suspension with random orientation can be expressed as:

$$I(q) = NV^2 \Delta\rho^2 P(q) S(q) \qquad (1)$$

where N is the number density of particles, V their volume, Δρ the difference of scattering length density between the solvent and the particle, P(q) the form factor of the particle, and S(q) the structure factor of interaction between the particles. The form factor describes the shape of the particle and the structure factor accounts for the interaction between them. The above

factorization is strictly applicable only for monodisperse and spherically symmetric particles. In this study, we are primarily dealing with dilute systems, hence the interaction between particles can be considered negligible and $S(q) \approx 1$ over the q range of investigation. For the analysis of the form factor, we have considered different morphologies such as disks, cylinders, tori, spherical shells, and the coexistence between disks and shells or tori and shells during the formation of the ULVs. In the mixed micelles and bilayers of TDMAO and LPFO, the electron density is dominated by the perfluorinated surfactant chains (522 e$^-$ nm^{-3}) as compared to the tetradecyl chains (264 e$^-$ nm^{-3}) and water (334 e$^-$ nm^{-3}). Therefore particles are assumed to be uniform in electron density. This does not have a significant effect on the deduced mean radius but slightly underestimates the bilayer thickness, due to the fact that the shorter perfluorinated chains of high contrast are not filling the interior of the bilayers.

For a sphere of uniform electron density and radius R, $P(q,R)$ is given by the following expression,[42]

$$P(q, R) = F_0^2(q, R) = \left(\frac{3[\sin(qR) - qR\cos(qR)]}{(qR)^3} \right)^2 \quad (2)$$

where $F_0(q,R)$ is the scattering amplitude of a sphere given by the Fourier transform of the radial electron density.

In the case of core–shell spheres with core and shell radii R_1 and R_2, respectively, the form factor depends on the contrasts of both core and shell:[43]

$$\Delta\rho^2 V^2 P(q, R_1, R_2) = [\Delta\rho_2 V_2 F_0(qR_2) - \Delta\rho_1 V_1 F_0(qR_1)]^2 \quad (3)$$

where $\Delta\rho_1$ and $\Delta\rho_2$ are the difference of scattering length densities between the core and the shell, and the solvent and the shell, respectively. For unilamellar vesicles, the core is filled with water and the resulting shell scattering function is given by:[15]

$$V^2 P(q, R_1, R_2) = \frac{16\pi^2}{9} \left[R_2^3 F_0(qR_2) - R_1^3 F_0(qR_1) \right]^2 \quad (4)$$

For the analysis presented, the scattering length density is assumed to be uniform across the bilayer. This is reasonable because LPFO and TDMAO chains mix well and no segregation of chains is expected, the interaction parameter β for this surfactant mixture has been determined to be −12 kT,[39] i.e., these are strongly synergistic mixtures. In addition, due to their low contrast, the scattering contribution of counterions (both Li$^+$ and OH$^-$) can be neglected. Moreover, the packing difference between the inner and outer layers of the bilayer is unlikely to make a significant difference in the scattering function of ULV.[44]

For disk-like and cylindrical micelles, $P(q,R,H)$ is given by the following expression:[42]

$$P(q, R, H) = \int_0^{\pi/2} \left\{ \left[\frac{2 J_1(qR\sin\alpha)}{qR\sin\alpha} \right] \left[\frac{\sin((qH/2)\cos\alpha)}{(qH/2)\cos\alpha} \right] \right\}^2 \sin\alpha d\alpha \quad (5)$$

where R and H are the radius and height of the cylinder or disk, α is the angle between the axis of the cylinder and the q direction, and J_1 represents the first order Bessel function. In the case of randomly oriented cylinders or disks, the integration is carried over all possible orientations with respect to q. Eqn (5) can be

extended to the core–shell morphology using eqn (3). When the cylinder has an elliptical cross-section with major and minor radii, a and b, respectively, $P(q)$ has the following form:[41]

$$P(q, R, H) = \frac{2}{\pi} \int_0^{\pi/2} \int_0^{\pi/2} \left\{ \left[\frac{2J_1(qr(a,b,\phi)\sin\alpha)}{qr(a,b,\phi)\sin\alpha} \right] \right.$$
$$\left. \times \left[\frac{\sin((qH/2)\cos a)}{(qH/2)\cos a} \right]^2 \right\} d\phi \sin\alpha d\alpha \quad (6)$$

where $r(a, b, \phi) = \sqrt{a^2\sin^2\phi + b^2\cos^2\phi}$.

The form factor of a torus with elliptical cross-section is given by the following expression:[45]

$$P(q, r, \gamma) = \int_0^{\pi/2} \left[\int_{c-a}^{c+a} \frac{2\pi r J_0(qr\sin\alpha)\sin(q\gamma\cos\alpha)}{q/2\cos\alpha} dr \right]^2 \sin\alpha d\alpha \quad (7)$$

where $\gamma = (b/a)\sqrt{a^2 - (r - c)^2}$ with a and b are major and minor radii of the elliptical cross-section and c is the distance from the origin to the center of the oblate cross-section and J_0 is the Bessel function of zeroth order.

The above expressions of scattering functions are applicable only to monodisperse systems. In order to account for the size distribution of micelles and vesicles, scattering functions need to be convoluted by the corresponding size distribution. For convenience, the polydispersity (p) of cylinders and disks is described by a Gaussian distribution function and a Schulz distribution was used in the case of vesicles. For tori, $P(q)$ already involves a double integral and the size distribution is coupled to the orientation distribution of the constituting cylinders and therefore a monodisperse function was assumed. The instrument resolution effect ($\Delta q \approx 10^{-2}$ nm^{-1} for sample-to-detector distance of 2.5 m) is not significant for the polydisperse systems involved here. The polydisperse intensity is given by the following general expression,[41]

$$I(q) = N \int_0^\infty \Delta\rho^2 V^2 P(q, R) f(R) dR \quad (8)$$

where $f(R)$ is the size distribution function (either Gaussian or Schulz). During the transformation process of disk-like or cylindrical micelles to vesicles, two morphologies coexist over the intermediate time period. In such cases, $I(q)$ can be decomposed into partial intensities of the components as $I_1(q)$ (e.g. disks) and $I_2(q)$ (vesicles).[15]

$$I(q) = \varphi I_1(q) + (1 - \varphi) I_2(q) \quad (9)$$

where φ is a relative volume fraction of the disks in the ensemble of vesicles and disk-like micelles. To model the data, different polydisperse form factors have been implemented in a MatLab program. This program enables the fitting of one dimensional normalized SAXS data.

3. Results

In this section, we describe the analysis of SAXS data and the underlying structural transformations at two different

concentrations following rapid mixing of the surfactant solutions. In order to compare with previous studies,[14,15] first we present the result of self-assembly process for a concentration of 25 mM of initial surfactants and then contrast with the observations for a lower concentration of 8 mM. In each case, we investigated the influence of the mixing ratio of the surfactant compositions on the final state of the system with the aim of finding ULVs with a narrow size distribution. Then we investigated the kinetic steps involved in the transformation process of initial surfactant solution to ULVs. Fig. 1 shows the SAXS intensities from the initial surfactant solutions of 8 mM and 25 mM. LPFO does not show any signature of micelles at these concentrations (micellar feature appears above 25 mM as shown in Fig. S1†). The TDMAO scattering curves can be modeled by core–shell cylinders of mean core radius 1.56 nm, shell thickness 0.30 nm and length 10.6 nm with $\Delta\rho_1$ and $\Delta\rho_2$ -3.6×10^{-4} nm^{-2} and 1.6×10^{-4} nm^{-2}, respectively. This leads to a radius of 1.86 nm for the cylindrical micelles and it is consistent with the previous report.[15]

3.1 Influence of the surfactant ratio on the vesicle structure

3.1.1 At moderate concentration (25 mM). In the previous studies, the dynamics of vesicle formation in similar systems was probed for equimolar mixing ratios of the surfactants in the range of 50–100 mM.[10,14,15] In this work, we first investigated the influence of the surfactant mixing ratio on the final state reached by the system within a few tens of seconds, where the phase behavior and structure at higher concentration have been studied previously.[38,39] ULVs are observed over an extended range in the phase diagram and the size of vesicles increases with increasing content of TDMAO.[38,39]

Fig. 2 shows the scattered intensity for 4 different ratios of TDMAO and LPFO for a total concentration of 25 mM for both surfactants with the relative mole fraction of TDMAO in the mixture x[TDMAO] varying from 0.4 to 0.57. From the shift in the position of the first minimum of the bilayer form factor from 1.35 to 1.2 nm^{-1} it is evident that the bilayers thickness increases with the addition of the longer chain TDMAO. When the mixing is equimolar and for excess of LPFO, the scattering curves can be described by a spherical shell function [eqn (4)] corresponding to
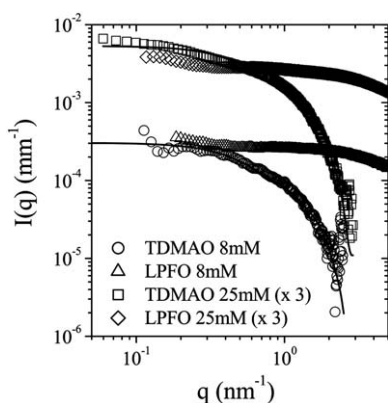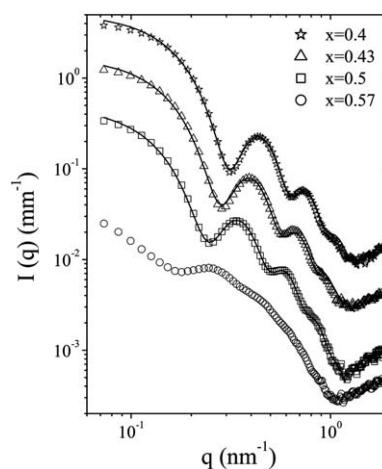
Fig. 2 SAXS intensities of the final state at different TDMAO fractions, x[TDMAO], of initial 25 mM solutions of TDMAO and LPFO. Successive curves have been multiplied by a factor 3 for clarity.

the formation of ULVs. The model curves for x[TDMAO] = 0.4, 0.43 and 0.5 correspond to radii of 11.4 nm, 12.5 nm and 14.4 nm and bilayer thicknesses of 3.5 nm, 3.65 nm, and 3.9 nm, respectively with a mean polydispersity of 0.07.

When TDMAO is in excess, the scattering curves display weaker features of shell scattering and the characteristic form factor minimum is shifted to lower q, indicating larger sized vesicles, which is in agreement with other observations at a higher concentration.[39] The scattering curve still has a minimum that corresponds to the vesicle form factor but with a larger polydispersity and size. Furthermore, it is quite likely that the system is in a structurally coexisting region, where ULVs are in equilibrium with rod-like micelles.[39] However, the lack of a Guinier region makes the modeling less reliable for such a two phase system and it is also of not direct interest in our studies.

3.1.2 At lower concentration (8 mM). Fig. 3 displays the scattered intensity for the final state at 6 different x[TDMAO] values from 0.33 to 0.6 for an initial surfactant concentration of 8 mM. As in the previous case at 25 mM, the scattering curves can still be described by a spherical shell function when the mixing is equimolar and LPFO is in excess. The system is in a unilamellar vesicle state with the mean radius of vesicles and the bilayer thickness increasing with the content of TDMAO in the mixture. The model curves for x[TDMAO] = 0.33, 0.4, 0.43 and 0.5 correspond to radii of 12.1 nm, 12.4 nm, 13.4 nm and 14.1 nm and bilayer thicknesses of 3.7 nm, 3.7 nm, 3.9 nm and 4.1 nm, respectively with a mean polydispersity of 0.09. On the other hand, when the TDMAO is in excess the scattering curves are lower in intensity and showing less pronounced features. Their shape cannot be modeled by a vesicle form factor and could correspond to an elongated structure, e.g., rod-like micelles similar to pure TDMAO.[14,20] In addition, a small constant background ($\sim 10^{-4}$ mm^{-1}) was required to describe the data at high q values. This is supposedly the signature of some free surfactant (LPFO) chains remaining in the solution in addition to ULVs, which enhance the solvent compressibility and thereby the background scattering level.

Fig. 1 Scattering from individual surfactant solutions of LPFO and TDMAO for the two concentrations reported. The scattering curves for 25 mM have been multiplied by a factor 3 for clarity.
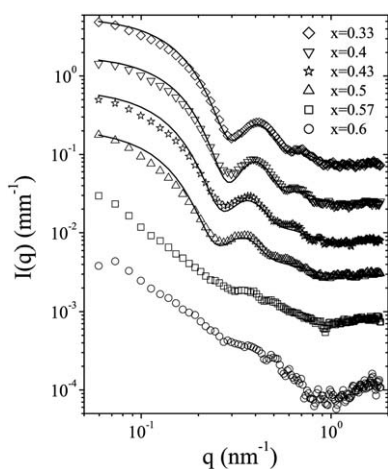
Fig. 3 SAXS intensities of the final state at different TDMAO fractions, *x*[TDMAO], of initial 8 mM solutions of TDMAO and LPFO. Successive curves have been multiplied by a factor 3 for clarity.

From the results above, it is clear that a narrower distribution of ULV is obtained when *x*[TDMAO] is lower than 0.5. Due to the high monomer solubility of LPFO, an excess of LPFO is required to retain the same composition of the bilayer as also observed at higher concentration.

3.2 Pathway for the formation of ULV

3.2.1 At moderate concentration (25 mM). Based on the above observations, we have chosen *x*[TDMAO] = 0.43 to investigate the pathway of the self-assembly process as this ratio exhibits the narrowest distribution of ULV size at equilibrium. The two surfactant solutions of initial concentration 25 mM were mixed rapidly using the stopped-flow device and the evolution of scattering patterns were followed during the first few seconds. Fig. 4 shows the time evolution of the scattered intensity between 2.3 ms and 3000 ms, the time range over which the main evolution of ULV is completed. Note that the first frame is taken before the cessation of the flow and the kinetic time at this stage is the dead time of the stopped-flow device (2.3 ms).
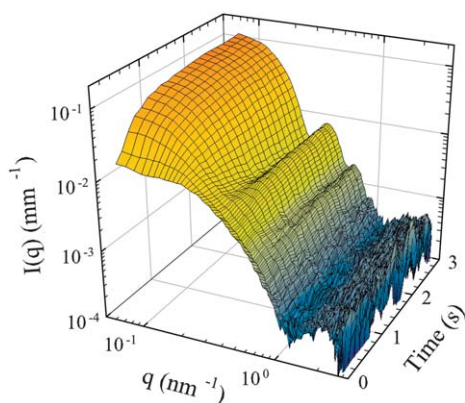

Fig. 4 Time evolution of the background subtracted scattered intensity upon mixing 25 mM solutions of TDMAO and LPFO in a 3 : 4 mixing ratio (*x*[TDMAO] = 0.43).

Fig. 5 presents the analysis of the representative scattering curves. The first curve at 2.3 ms can very well be described by a disk-like scattering function [eqn (8) with eqn (5)] resulting in a mean radius of approximately 6.0 nm and bilayer thickness of about 4.0 nm, which corresponds to a total aggregation number of 490 as estimated from the volume. These disk-like micelles then grow for about 200 ms to reach a radius of 10.0 nm and still have a thickness of 4.0 nm. From then on, disk-like micelles close to form unilamellar vesicles which are described by eqn (4) and (8). This process lasts for about 3 seconds and the final ULV have a mean radius of 12.5 nm and a bilayer thickness of 3.6 nm consistent with the static measurement. During the transformation of the disk-like micelles to ULV, both these structural moieties coexist. Therefore, *I*(*q*) was decomposed into two components using eqn (9). This allowed us to deduce the relative fraction by volume (*φ*) of disk-like micelles and ULVs. Fig. 6 shows that *φ* decays with time (*t*) roughly by an exponential function given by, $\varphi = 1.18 \exp^{(-t/0.76)}$.

This type of kinetics is the same as that observed in previous studies for solutions at higher surfactant concentrations (50 mM) and equimolar mixing ratio.[15] In the present case, the initial concentration is well above the cmc of TDMAO and just below that of LPFO, which means that also for the LPFO a smaller fraction of the surfactant is already present in premicellar aggregates. In addition, the cmc of the mixed surfactant system is substantially lower than the individual cmc's due to strong synergy between LPFO and TDMAO.[38] For instance, the mixed cmc (or critical vesicular concentration) drops rapidly from pure LPFO cmc in the presence of TDMAO.[38] Furthermore, the mixed cmc remains nearly constant at about 0.06 mM for *x*[TDMAO] range of 0.2–0.8. Therefore, the system exhibits a strong tendency to form disk-like mixed micelles as at higher concentrations and they are already formed within the mixing process (<2.3 ms). The initially observed disk-like micelles are already mixed micelles of TDMAO and LPFO formed during the
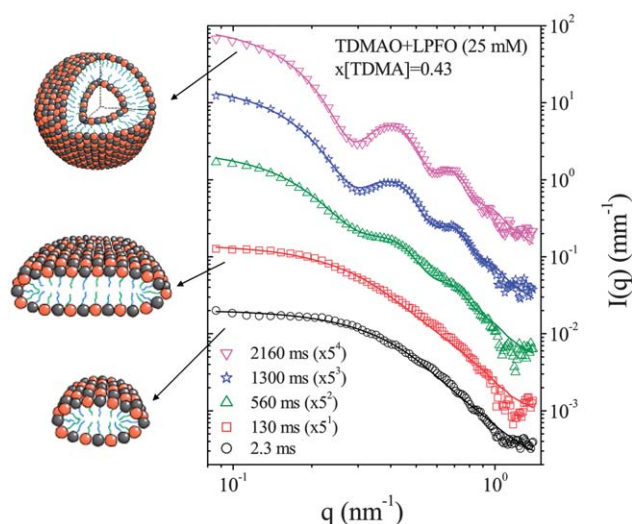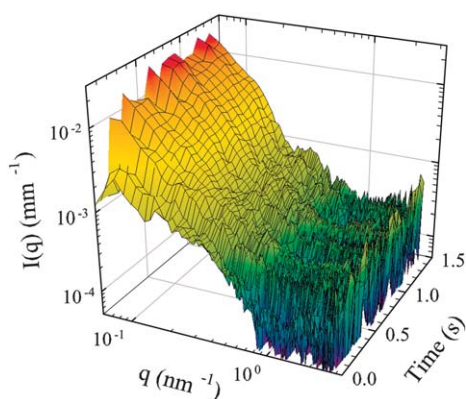

Fig. 5 Representative time-resolved SAXS intensities after mixing of 25 mM solutions of TDMAO and LPFO with *x*[TDMAO] = 0.43. Successive curves have been multiplied by a factor 5 for clarity. The continuous lines correspond to models described in the text. The cartoons illustrate the different aggregate shapes used to model the data.
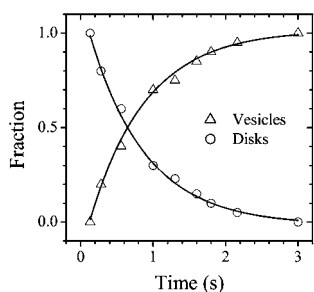
Fig. 6 Time evolution of the fraction of disk-like micelles and ULVs during the conversion process illustrated in Fig. 4.

mixing process.[15] These disk-like micelles are characterized by an unfavourable edge-energy and to minimize it, disks grow within the first second and subsequently close to form ULVs. The main difference is that intermediate disk-like micelles and ULVs are slightly smaller in their size and the kinetics of their transformation seems to be faster by about a factor 2 than in the 50 mM equimolar case. The ULVs are in a metastable state and they grow in size and their distribution becomes wider over time scales of hours.

3.2.2 At lower concentration (8 mM). In the following, we present the observations for a sample of 8 mM total concentration and x[TDMAO] = 0.43, the optimum ratio for the formation of well-defined ULVs (see Section 3.1.2). The solutions of initial surfactant components were again mixed using the stopped-flow device and the scattering patterns were recorded during the self-assembly process. Fig. 7 illustrates the evolution of scattered intensity between 2.3 ms and 1500 ms, the period over which the ULV formation is completed. Qualitatively the scattering curves show different features than in Fig. 4. Nevertheless, the final state is suggestive of formation of polydisperse ULVs. The low q features of initial scattering patterns are indicative of the presence of elongated structures. Fig. 8 presents the analysis of representative time-resolved scattering curves. Here, the first TDMAO–LPFO mixed micelles scattering curve can be modeled by a polydisperse cylinder as opposed to the disk-like mixed micelles in the 25 mM case. Note that pure TDMAO

Fig. 7 Time evolution of the background subtracted scattered intensity up on mixing 8 mM solutions of TDMAO and LPFO in a 3 : 4 ratio (x[TDMAO] = 0.43).
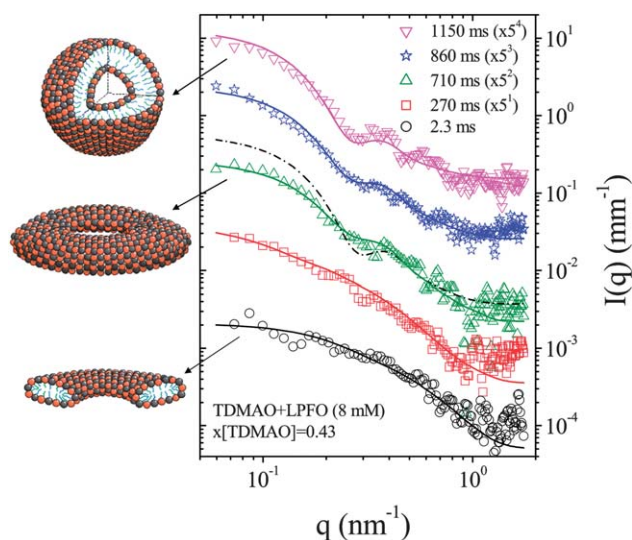
Fig. 8 Time evolution of SAXS intensities following the rapid mixing of initial 8 mM solutions with x[TDMAO] = 0.43. Successive curves have been multiplied by a factor 5 for clarity. The continuous and dashed-dotted lines for 710 ms represent model fits for torus and ULV, respectively. The cartoons illustrate the different aggregate shapes used to model the data.

micelles are also modeled by cylinder-like objects with radius and height 1.85 nm and 10.6 nm, respectively (Fig. 1). The mixed micelles at 2.3 ms correspond to a cylinder of mean length about 20 nm and radius of 2.7 nm. The apparent increase in the radius of the mixed micelles is not consistent with the length of the surfactant chains. However, this discrepancy can be eliminated by using a cylinder with an oblate elliptical cross-section to model the data [eqn (6)]. The resulting model parameters are length about 22.0 nm, major and minor radii 3.0 nm and 1.9 nm, respectively and polydispersity of major radius 0.2. The dimension of the minor axis is consistent with the length of the stretched TDMAO molecule (2.15 nm) and also corresponds well to the thickness of the bilayer observed in the final vesicles (3.9 nm). This size is substantially bigger than TDMAO cylindrical micelles, which implies that the original micelles of TDMAO have incorporated LPFO molecules (and probably another TDMAO micelle) during the short mixing time resulting in the formation of mixed micelles of the same morphology. By adapting an elliptical cross-section, the micellar aggregates are already accommodating the lower curvature preferred by the LPFO. However, this incorporation has to proceed *via* monomer diffusion, while at higher concentration it was facilitated *via* coalescence of micelles of the two different surfactants. The increase of the signal in the high q region is also an evidence for free perfluorinated chains in the solution and the intensity level is indicative of the relative concentration. During the formation process, the system is quite far away from equilibrium and therefore it has a higher effective chemical potential resulting in a much higher monomer concentration.

The cylindrical mixed micelles further grow to sizes longer than 40 nm and their Guinier region goes out of the q window in Fig. 8. The curve for 270 ms corresponds to length about 50.0 nm, major and minor radii 5.0 and 1.9 nm, respectively, *i.e.*,

the average curvature has decreased further during the growth process by incorporation of LPFO. At about 700 ms, the scattering curve changes to a different structure which appears more compact. This intermediate structure is different from ULVs and can be modeled with a torus-like form factor with elliptical cross-section [eqn (7)]. The parameters of the torus are radius about 10.0 nm, cross-sectional major and minor radii 6.0 nm and 1.9 nm, respectively. This corresponds to a torus perimeter of about 63 nm, suggesting that the cylinders grow until they reach this length and then they are flexible enough to close and form the torus-like structure. Finally, in a third step within one second, the tori merge to form ULVs with a mean radius of 13.4 nm and a bilayer thickness of 3.9 nm. These vesicles are somewhat more polydisperse ($p = 0.09$) but their size is very similar to the one observed for the higher concentrations (25 mM). At intermediate time, tori and ULV's coexist (*e.g.* at 860 ms the model curve in Fig. 8 represents a linear combination of 60% torii and 40% vesicles). This means that even if the pathway is different, the final structure is the same as in the concentrated case, which is a clear indication that there is a thermodynamic driving force for the formation of ULVs in these mixtures.[6,15] The obtained final state is consistent with the static measurements presented in Fig. 3.

An analogous behavior was also observed at 4 mM but in this case the quality of the data became less satisfactory for quantitative modeling. Longer exposure time was not allowed due to the onset of radiation damage. As a result, the total exposure time for a sequence had to be maintained below the threshold for radiation induced changes, as ascertained for all the data presented here.

4. Discussion

The results presented in the previous section illustrate that the mixed micellar system of TDMAO/LPFO can go through two different pathways to form unilamellar vesicles depending on the initial concentration of surfactants. The pathway for 25 mM case is similar to the one that has been observed for a higher concentration of surfactants above the cmc of LPFO.[14] It involves the fast formation of disk-like mixed micelles (by fast fusion of the originally present individual micelles) during the mixing process and these disks subsequently grow to a critical size beyond which they close to form ULVs. In this case, the growth of the disks and the subsequent formation of the vesicles is primarily driven by the need to reduce their unfavorable edge energy. Above a critical size, the bending energy becomes favorable for closure and formation of unilamellar vesicles.[7,11,12,15,46] At 25 mM though the system is just below the cmc of LPFO, the strong synergy between LPFO and TDMAO leads to formation of mixed micelles during the rapid mixing process. An apparent difference is that the growth of disk-like micelles and their conversion to ULVs is faster by about a factor 2 than in the 50 mM equimolar case. The difference can be attributed to a combination of variation in the mixing ratio, $x[\text{TDMAO}] = 0.43$, and that the maximum size of the disk-like micelles and the initially formed ULVs are smaller than in the equimolar case ($x = 0.5$).

The second pathway observed in the case of 8 mM total surfactant concentration involves the formation of cylindrical
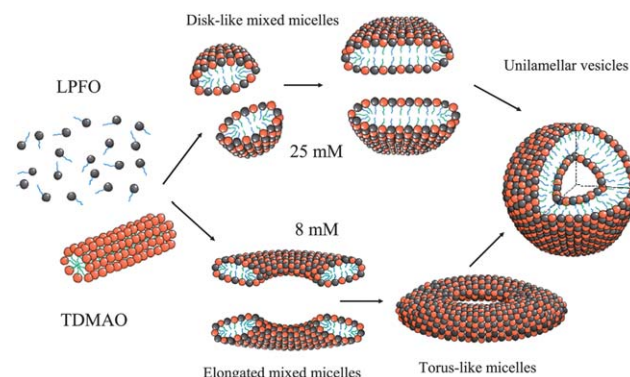
Fig. 9 Schematic representation of the two different pathways followed in the formation of ULVs near (25 mM) and well below (8 mM) the cmc of the anionic micelles (LPFO).

mixed micelles with an elliptical cross-section that fuse to form tori-like structures and finally transform to unilamellar vesicles (see Fig. 8). Here the system is clearly below the cmc of LPFO, free LPFO molecules interact with the rod-like TDMAO micelles and presumably incorporate molecule by molecule thereby decorate the rods progressively. This changes the spontaneous curvature of cylinders in a continuous fashion and the average curvature is systematically lowered by increasing the ellipticity of the cross-section. By the monomer addition process combined with end-to-end fusion, the cylindrical mixed micelles grow from about 20 nm length to over 60 nm during the first 700 ms. At this stage, the spontaneous curvature of cylinders becomes favorable to fold and form tori. The parameter values of the initially formed tori indicate that the cylinders are about 60 nm long before they fold and the bilayer thickness is similar to the initially formed mixed micelles. But the torus structure is a very unstable configuration in terms of the packing of surfactants, and its instability has been argued on the basis of their bending entropy.[47] In this state the curvature of the torus adds constraints on top of the packing as the cross-sectional radii of the tori are only about 6 nm and 1.9 nm. That may be why within the subsequent 300 ms the tori fuse and reorganize to form ULVs, which is finally the more energetically favorable configuration for the mixed system as seen in the previous studies. The overall pathway is schematically depicted in Fig. 9. Formation of torus-like intermediate structures and their fusion have also been seen in computer simulations of block-copolymer micellar self-assembly.[33,34] Rod-like and torus-like morphologies are also observed in micellar transformations under out-of-equilibrium conditions.[48,49]

5. Conclusion

Time-resolved small-angle X-ray scattering combined with rapid stopped-flow mixing method offers a powerful approach to probe self-assembly processes in amphiphilic systems in the millisecond range.[30] The high brilliance of the X-ray beam coupled with a high sensitivity CCD detector enabled us to access millisecond time resolution even for weakly scattering systems. This allowed us to investigate the zwitterionic–anionic surfactant mixtures of TDMAO and LPFO down to very low concentrations, where the LPFO is well below its cmc. Static SAXS

experiments showed that in the concentration range of 4 to 50 mM, unilamellar vesicles are formed over an extended range of mixing ratios. Smaller and less polydisperse vesicles are formed in the LPFO rich side while they become larger and less well-defined for high TDMAO content.

In the formation process, disk-like mixed micelles are observed as intermediate structures in the proximity of the cmc of LPFO and above, while elongated cylinders and tori are favored at lower concentrations. In the first pathway, the initially present disk-like micelles are formed by fusion of the two types of surfactant micelles thereby changing the composition of the mixed micelles in a jump-wise fashion and reaching the final average composition within the mixing time. These disks grow by a coalescence mechanism until reaching a given critical size beyond which they close to form well-defined zwitteranionic unilamellar vesicles as schematically depicted in Fig. 9. When the LPFO concentration is well below the cmc, the monomer addition mechanism seems to control the self-assembly process. The free LPFO molecules become incorporated into the TDMAO rod-like micelles thereby leading to a gradual change of composition and curvature. This is different from the situation at higher concentration where both surfactants micelles are initially present and their fusion leads to a rapid change of the composition and thereby immediately to conditions favourable for bilayers. For the case of low concentration, the rod-like TDMAO micelles adopt quickly an elliptical cross-section and then grow continuously by incorporation of individual LPFO molecules and also at the same time by fusion with other micelles to form longer micelles. Beyond a maximum length (about 60 nm), the long cylinders close to form tori. However, these tori are not long-time stable and close in a rather fast process (a few hundred milliseconds) to form ULVs. The overall process is always driven by the need for the system to adopt the most energetically favorable packing of two dissimilar surfactant molecules.

In summary, the most important finding is certainly that similar final structures can be obtained *via* quite different structural pathways, which opens up opportunities to manipulate the time scales and the formation process itself by appropriately choosing the system composition. This is also a further compelling proof for the thermodynamic stability of these unilamellar vesicles as they are approached and formed *via* quite different kinetic pathways, which in the end yield the same structures.

Acknowledgements

References

1 D. D. Lasic, R. Joannic, B. C. Keller, P. M. Frederik and L. Auvray, *Adv. Colloid Interface Sci.*, 2001, **89–90**, 337.
2 V. Guida, *Adv. Colloid Interface Sci.*, 2010, **161**, 77.
3 D. D. Lasic, Liposomes: from physics to application, Elsevier, Amsterdam, 1993.
4 *Vesicles, Surf. Science Series*, ed. M. Rosoff, Marcel Dekker, New York, 1996, vol. 62.
5 R. G. Laughlin, *The Aqueous Phase Behavior of Surfactants*, Academic Press, San Diego, CA, 1994.
6 H. T. Jung, B. Coldren, J. A. Zasadzinski, D. J. Iampietro and E. W. Kaler, *Proc. Natl. Acad. Sci. U. S. A.*, 2001, **98**, 1353.
7 H. T. Jung, S. Y. Lee, E. W. Kaler, B. Coldren and J. A. Zasadzinski, *Proc. Natl. Acad. Sci. U. S. A.*, 2002, **99**, 15318.
8 M. Gradzielski, *J. Phys.: Condens. Matter*, 2003, **15**, R655.
9 S. U. Egelhaaf and P. Schurtenberger, *Phys. Rev. Lett.*, 1999, **82**, 2804.
10 S. Schmölzer, D. Gräbner, M. Gradzielski and T. Narayanan, *Phys. Rev. Lett.*, 2002, **88**, 258301.
11 A. Shioi and T. A. Hatton, *Langmuir*, 2002, **18**, 7341.
12 J. Leng, S. U. Egelhaaf and M. E. Cates, *Biophys. J.*, 2003, **85**, 1624.
13 R. G. Laughlin, *Colloids Surf., A*, 1997, **128**, 27.
14 T. M. Weiss, T. Narayanan, C. Wolf, M. Gradzielski, P. Panine, S. Finet and W. I. Helsby, *Phys. Rev. Lett.*, 2005, **94**, 038303.
15 T. M. Weiss, T. Narayanan and M. Gradzielski, *Langmuir*, 2008, **24**, 3759.
16 I. Grillo, J. Penfold, I. Tucker and F. Cousin, *Langmuir*, 2009, **25**, 3932.
17 E. Di Cola, C. Lefebvre, A. Deffieux, T. Narayanan and R. Borsali, *Soft Matter*, 2009, **5**, 1081.
18 F. Li, S. Prevost, R. Schweins, A. T. M. Marcelis, F. A. M. Leermakers, M. A. Cohen Stuart and E. J. R. Sudhölter, *Soft Matter*, 2009, **5**, 4169.
19 Y. Han, H. Yu, H. Du and J. Jiang, *J. Am. Chem. Soc.*, 2010, **132**, 1144.
20 K. Bressel, M. Muthig, S. Prévost, I. Grillo and M. Gradzielski, *Colloid Polym. Sci.*, 2010, **288**, 827.
21 K. Bryskhe, S. Bulut and U. Olsson, *J. Phys. Chem. B*, 2005, **109**, 9265.
22 B. F. B. Silva, E. F. Marques and U. Olsson, *Langmuir*, 2008, **24**, 10746.
23 N. Micali, V. Villari, G. M. L. Consoli, F. Cunsolo and C. Geraci, *Phys. Rev. E*, 2006, **73**, 051904.
24 L. Shen, J. Du, S. P. Armes and S. Liu, *Langmuir*, 2008, **24**, 10019.
25 E. A. G. Aniansson, S. N. Wall, M. Almgren, H. Hoffmann, I. Kielmann, W. Ulbricht, R. Zana, J. Lang and C. Tondre, *J. Phys. Chem.*, 1976, **80**, 905.
26 H. Noguchi and G. Gompper, *J. Chem. Phys.*, 2006, **125**, 164908.
27 A. J. O'Connor, T. A. Hatton and A. Bose, *Langmuir*, 1997, **13**, 6931.
28 P. Panine, S. Finet, T. M. Weiss and T. Narayanan, *Adv. Colloid Interface Sci.*, 2006, **127**, 9.
29 I. Grillo, *Curr. Opin. Colloid Interface Sci.*, 2009, **14**, 402.
30 T. Narayanan, *Curr. Opin. Colloid Interface Sci.*, 2009, **14**, 409.
31 R. Lund, L. Willner, M. Monkenbusch, P. Panine, T. Narayanan, J. Colmenero and D. Richter, *Phys. Rev. Lett.*, 2009, **102**, 188301.
32 X. He and F. Schmid, *Macromolecules*, 2006, **39**, 2654.
33 X. He and F. Schmid, *Phys. Rev. Lett.*, 2008, **100**, 137802.
34 P. He, X. Li, D. Kou, M. Deng and H. Liang, *J. Chem. Phys.*, 2010, **132**, 204905.
35 E. W. Kaler, K. L. Herrington, A. K. Murthy and J. A. Zasadzinski, *J. Phys. Chem.*, 1992, **96**, 6698.
36 S. A. Safran, P. A. Pincus, D. Andelman and F. C. MacKintosh, *Phys. Rev. A*, 1991, **43**, 1071.
37 E. F. Marques, O. Regev, A. Khan, M. G. Miguel and B. Lindman, *J. Phys. Chem. B*, 1998, **102**, 6746.
38 C. Wolf, K. Bressel, M. Drechsler and M. Gradzielski, *Langmuir*, 2009, **25**, 11358.
39 K. Bressel, S. Prévost, B. Tiersch, J. Koetz, and M. Gradzielski, 2009, submitted.
40 H. Hoffmann, M. Bergmeier, M. Gradzielski and C. Thunig, *Prog. Colloid Polym. Sci.*, 1998, **109**, 13.
41 J. S. Pedersen, in *Neutrons, X-Rays and Light: Scattering Methods Applied to Soft Condensed Matter*, ed. P. Lindner and T. Zemb, Elsevier, Amsterdam, 2002, p. 391.
42 A. Guinier and G. Fournet, *Small-Angle Scattering of X-Rays*, Wiley, New York, 1955.
43 P. Bartlett and R. H. Ottewill, *J. Chem. Phys.*, 1992, **96**, 3306.
44 N. Kucerka, J. F. Nagle, S. E. Feller and P. Balgavy, *Phys. Rev. E*, 2004, **69**, 051903.
45 T. Kawaguchi, *J. Appl. Crystallogr.*, 2001, **34**, 580.
46 P. Fromherz, *Chem. Phys. Lett.*, 1983, **94**, 259.
47 G. Porte, *J. Phys. Chem.*, 1983, **87**, 354.
48 Y. Kawabata, T. Shinoda and T. Kato, *Phys. Chem. Chem. Phys.*, 2011, **13**, 3484.
49 Z. Wang and W. Jiang, *Soft Matter*, 2010, **6**, 3743.